Distinct guard cell specific remodeling of chromatin accessibility during abscisic acid and CO_2 dependent stomatal regulation

Authors
Charles A. Seller[1*] and Julian I. Schroeder[1*]

Affiliations
1. School of Biological Sciences
Cell and Developmental Biology Department
University of California San Diego,
La Jolla, CA 92093-0116
*Corresponding authors. Email: cseller@ucsd.edu; jischroeder@ucsd.edu

Classification: Plant Biology

Keywords: Guard cells, stomata, chromatin, plant hormones, abscisic acid, transcription factors, carbon dioxide

Abstract

In plants, epidermal guard cells integrate and respond to numerous environmental signals to control stomatal pore apertures thereby regulating gas exchange. Chromatin structure controls transcription factor access to the genome, but whether large-scale chromatin remodeling occurs in guard cells during stomatal movements, and in response to the hormone abscisic acid (ABA) in general, remain unknown. Here we isolate guard cell nuclei from *Arabidopsis thaliana* plants to examine whether the physiological signals, ABA and CO_2, regulate guard cell chromatin during stomatal movements. Our cell type specific analyses uncover patterns of chromatin accessibility specific to guard cells and define novel cis-regulatory sequences supporting guard cell specific gene expression. We find that ABA triggers extensive and dynamic chromatin remodeling in guard cells, roots, and mesophyll cells with clear patterns of cell-type specificity. DNA motif analyses uncover binding sites for distinct transcription factors enriched in ABA-induced and ABA-repressed chromatin. We identify the ABF/AREB bZIP-type transcription factors that are required for ABA-triggered chromatin opening in guard cells and implicate the inhibition of a set of bHLH-type transcription factors in controlling ABA-repressed chromatin. Moreover, we demonstrate that ABA and CO_2 induce distinct programs of chromatin remodeling. We provide insight into the control of guard cell chromatin dynamics and propose that ABA-induced chromatin remodeling primes the genome for abiotic stress resistance.

Significance statement

Specialized leaf cells called guard cells integrate environmental cues to optimally control the size of microscopic stomatal pores. The hormone abscisic acid (ABA), a key regulator of plant drought responses, and changes in atmospheric CO_2 concentration are signals that control stomatal aperture size, but whether these signals also regulate genome packaging into chromatin is unknown. Using guard cell specific chromatin profiling we uncovered regulatory DNA sequences driving specific gene expression in this cell-type. We also discovered that ABA triggers extensive and persistent changes to chromatin structure in guard cells. Unexpectedly, exposure of plants to elevated atmospheric CO_2 had only minimal impact on chromatin dynamics. Furthermore, we identified the specific transcription factors that regulate ABA-induced chromatin dynamics in guard cells.

INTRODUCTION

Organisms evolved mechanisms that connect the activity of their genome to the conditions in their environment. Developmental and environmental signals can impact the genome by regulating transcription factor (TF) binding to cognate DNA sequences known as cis-regulatory elements (CRE) (1). In eukaryotes, this regulation occurs in the context of chromatin where nucleosomes can impede transcription factor binding to target sequences (2, 3). Consequently, the remodeling of chromatin structure to allow access of transcription factors to target DNA is thought to be a key step in gene regulation. Plant hormones are key signaling molecules controlling numerous aspects of plant life that coordinate genome activity with environmental conditions (4, 5). Recent studies have provided insight into how chromatin structure changes during plant development (6–12) and in response to environmental and hormonal stimuli (13–15).

Here we focus on the abscisic acid (ABA) signal transduction pathway to explore the connection between hormone signaling and chromatin structure in plants. ABA is a major plant stress hormone that accumulates in cells and tissues experiencing abiotic stress, especially those linked to plant water-status (16–18). ABA signals through a well understood core module consisting of PYR/PYL/RCAR ABA receptor proteins, PP2C protein phosphatases, and SnRK2 protein kinases (19–21). Upon ABA binding, PYR/PYL/RCAR receptor proteins inactivate PP2C phosphatases resulting in the derepression of SnRK2 kinases. ABA-activated SnRK2 kinases then phosphorylate and thereby directly regulate downstream proteins including numerous transcription factors (22–28). Consequently, ABA triggers the differential expression of thousands of genes in the *Arabidopsis thaliana* genome (4, 29–31). However, it remains unclear, especially at the genome scale, whether ABA signaling reshapes chromatin structure, and how ABA-regulated TFs might function in the context of chromatin.

78 One well known action of ABA is to trigger the closure of the stomatal aperture (17). Stomata
79 are small pores on the surface of the leaf that mediate gas exchange and are formed by a pair
80 of specialized epidermal cells known as guard cells. Guard cells perceive and respond to
81 multiple environmental and hormonal cues in order to optimally regulate the size of the stomatal
82 pore (32–34). For instance, some signals such as elevated atmospheric carbon dioxide (CO_2),
83 ABA, and the immune elicitor Flg22 trigger stomatal closure, while reduced CO_2, light, and heat
84 trigger stomatal opening. Because of their exquisite environmental reactivity, guard cells are an
85 excellent model cell system to investigate how different physiological signals regulate chromatin
86 structure in a cell-type specific manner. Although the recent application of single-cell RNA-seq
87 to *Arabidopsis* has expanded our understanding of gene regulation, these studies often focus on
88 plate-grown seedlings (35, 36) and/or resulted in datasets with limited representation of guard
89 cells (37, 38). To apply epigenomic techniques to the question of how guard cells respond to
90 different stimuli new protocols are needed that can isolate large numbers of pure guard cells
91 from soil grown plants, a more relevant setting for physiological studies.
92
93 In this paper, we describe the development of an approach to purify guard cell nuclei and by
94 deploying this method, uncover how guard cell chromatin structure changes in response to
95 different stimuli that drive stomatal movements. We profiled the chromatin and transcriptional
96 reprogramming in response to ABA in three different developmental contexts – roots, mesophyll
97 cells, and guard cells. We map thousands of loci that gain or lose chromatin accessibility in
98 response to ABA and link these regions to co-regulated transcripts, uncovering a critical role for
99 chromatin dynamics in controlling ABA-dependent transcription. Furthermore, we show that
100 genome-wide and persistent changes to chromatin structure accompany ABA-induced stomatal
101 closure and that four related bZIP transcription factors known as ABRE Binding Factors (ABFs)
102 are required for initiating the majority of ABA-induced chromatin opening. In contrast, we
103 implicate a family of related bHLH-type TFs known as ABA-Kinase Substrates (AKSs) in the

maintenance of open chromatin upstream of ABA-repressed genes. Finally, we show that in guard cells, changes to atmospheric CO_2-concentration trigger distinct and more limited chromatin remodeling and gene regulatory programs from those mediated by abscisic acid.

RESULTS

ABA induces rapid and genome-wide chromatin remodeling in roots

As an initial test of the relationship between ABA and chromatin we focused on *Arabidopsis thaliana* seedlings. To measure changes to chromatin structure we combined fluorescence activated nuclei sorting (FANS) with the Assay for Transposase-Accessible Chromatin with sequencing (ATAC-seq), a quantitative measurement of chromatin accessibility across the genome (39, 40). 50,000 nuclei per sample were isolated using FANS (Fig. S1A). We called 25,753 ATAC-seq peaks across all whole seedling and seedling root libraries (Datasets S1 and S2). Genomic regions coinciding with these peaks are known as Accessible Chromatin Regions (ACRs) and predominantly aligned with upstream regulatory regions in the genome (Fig. S1B-E). In contrast, ATAC-seq reads derived from purified genomic DNA did not cluster into defined peaks (Fig. S1B,C). We next treated whole seedlings with ABA and profiled chromatin accessibility after 4 hours. Differential analysis revealed hundreds of regions that significantly gain and lose accessibility in response to ABA (Fig. 1A, Dataset S3).

To capture the dynamics of ABA-induced chromatin remodeling we focused on roots which can rapidly take up ABA from their surroundings (41, 42). Using FANS, we isolated root nuclei at three different timepoints following ABA treatment (after 45, 120, and 240 minutes) and performed ATAC-seq. Differential analysis revealed that ABA triggers time-dependent changes in chromatin accessibility in roots (Dataset S3). Heatmaps centered over these ABA regulated ACRs illustrate the progressive impact of ABA on chromatin structure, with more regions of the

130 genome changing in ATAC-signal over time (Fig. 1B,C). We observed significant changes to
131 chromatin after only 45 minutes of ABA treatment, with 163 ACRs located in upstream
132 regulatory regions gaining accessibility and 64 losing accessibility (Fig. 1C,E). After 4 hours,
133 ABA had activated 1293 ACRs and repressed 1119 ACRs (Dataset S3). Interestingly, we found
134 that ABA-regulated ACRs tend to be located further away from transcription start sites (> 1kb)
135 than static regions (Fig. 1D). ABA-induced ACRs were associated with downstream genes
136 enriched for gene ontology (GO) terms such as “response to water deprivation”, “response to
137 osmotic stress”, and “response to abscisic acid” (Dataset S6).
138
139 To explore the role of specific transcription factors in orchestrating these changes we performed
140 DNA motif analysis using a set of motifs empirically generated by the in vitro DNA binding assay
141 DAP-seq (43). We found that motifs recognized by ABF/AREB transcription factors such as
142 ABF1/2/3/4 and ABI5 were highly enriched in ABA-induced ACRs (Fig. 1F, example ABF1, p =
143 1e-63, Dataset S7). In contrast, we found that ABA-repressed ACRs showed enrichment for
144 motifs recognized by the related bHLH type transcription factors AKS1, AKS3, and bHLH80
145 (Fig. 1F, example AKS3, p = 1e-32, Dataset S7). Notably, both ABF1/2/3/4 and AKS1/2/3
146 proteins are direct targets of ABA-regulated SnRK2 kinases (22, 24). Previous research has
147 shown a role for ABA-dependent inhibition of bHLH-type AKS transcription factors in the
148 transcriptional repression of the guard cell K^+ channel *KAT1* (24, 44). Interestingly, our findings
149 suggest a larger role for the AKS clade of closely related bHLH proteins in the regulation of
150 ABA-repressed genes. We conclude that ABA can trigger rapid and genome-wide chromatin
151 remodeling in root tissue.
152
153 **Revealing guard cell specific patterns of chromatin accessibility**
154 Encouraged by our findings in whole seedlings and roots we next decided to investigate the
155 effect of ABA on chromatin in mature guard cells. We first developed a FACS-based strategy to

purify guard cell nuclei from soil-grown plants. Nuclei were labeled by expressing the histone H2B fused to GFP under the control of the guard cell *pGC1* promoter (45). We first confirmed the guard cell specificity of the H2B-GFP fusion in our transgenic lines using fluorescence microscopy (Fig. 2A) and confirmed that ABA treatment did not alter the guard cell specific expression (Fig. S2A). We first isolated nuclei from leaf epidermal samples harvested from *GC1:H2B-GFP* plants. DAPI stained nuclei preparations were then analyzed using FACS (Fig S2B). We could define a clearly separated GFP-positive population among all detected nuclei (Fig. 2B, Fig. S2C). In contrast to many other cell types in the *Arabidopsis* leaf, guard cells are diploid, and GFP-positive nuclei from *pGC1:H2B-GFP* expressing plants had a 2n DNA content while GFP-negative nuclei were distributed among higher ploidy levels (Fig. 2C). Approximately 5% of GFP-positive particles (41 out of 5037 total from a single FACS run) had DAPI content greater than 2N, however we sorted only 2N nuclei for downstream applications. This method allowed us to obtain ~30,000 guard cell nuclei with an estimated purity of 98% (Fig. S2D) from the leaves of 40-50 plants. To assay guard cell chromatin structure, nuclei isolated using this method were used to generate ATAC-seq libraries. The resulting libraries were of high quality with clear concentration of peaks in annotated upstream regulatory regions (Fig. S2E), enrichment of open chromatin fragments (< 100 bp) immediately upstream of transcription start sites (Fig. S2F), strong correlation between biological replicates (Fig. S2G), and high FRiP (fraction of reads in peaks) scores (Dataset S1).

In parallel, we generated ATAC-seq samples from root nuclei and from FANS-isolated mesophyll nuclei labeled by expression of H2B-GFP from the promoter of the mesophyll expressed Rubisco small subunit 2B gene (Fig. S3A-C) (6). For each tissue/cell-type we compared ATAC-seq libraries derived from three biological replicates. We identified 30,985 ATAC-seq peaks across all samples (Dataset S2) and called cell-type enriched peaks using pairwise differentially accessibility analysis. Although most ATAC-seq peaks did not differ

182 significantly among cell types, we found 3272 guard cell enriched ACRs, 1472 mesophyll
183 enriched ACRs, and 3364 root enriched ACRs (Dataset S2). Heatmaps centered over these
184 regions highlight characteristics of cell/tissue specificity in the observed patterns of chromatin
185 accessibility (Fig. 2D, Fig. S4A). Importantly, biological replicates derived from the same
186 tissue/cell-type clustered together in principal component analysis (PCA) underscoring the
187 robustness of this approach (Fig. 2E).
188
189 To evaluate the relationship between guard cell enriched chromatin accessibility and gene
190 expression we performed RNA-seq on both whole leaves and guard cell-enriched samples. We
191 found that regions with high chromatin accessibility specifically in guard cells were associated
192 with elevated transcript levels from the adjacent downstream genes, indicating that we are
193 identifying functional cis-regulatory elements (CREs) (Fig. 2F). Although the overall correlation
194 between promoter chromatin accessibility and downstream transcript level was weak in guard
195 cells (r = 0.19, Fig. S4B), we found that differentially accessible ACRs were more strongly
196 correlated with downstream gene differential expression (r = 0.58, Fig. S4C). Examination of
197 individual gene loci like the guard cell expressed gene *KAT1* (46–48) illustrated the connection
198 between increased upstream accessibility and increased transcript levels (Fig. 2G and Fig
199 S4D). By contrast, the mesophyll expressed gene *AOC1* showed had high chromatin
200 accessibility in mesophyll cells, but minimal upstream ATAC-seq signal in guard cells (Fig. 2G).
201 TF binding motif analysis on guard cell enriched ACRs returned de novo motifs with strong
202 similarity to motifs recognized by known stomatal lineage transcriptional regulators such as the
203 bHLH proteins SPCH, MUTE, and FAMA as well as EDT1 and DOF-type TFs (49–53) (Fig. 2H
204 and Dataset S7). In contrast, we find that WRKY-type TF binding motifs are enriched in regions
205 with that are significantly less accessible in guard cells compared to roots and mesophyll cells
206 (Table S7). However, these motifs are recognized by large transcription factor families
207 containing many transcription factors that are not specific to guard cells, for instance SPCH and

208 MUTE are active only early during stomatal lineage development (49, 50). By connecting guard
209 cell specific ACRs with downstream guard cell enriched transcripts we were able to define a set
210 of 827 putative regulatory elements preferentially active in guard cells (Table S4). To further
211 confirm that our approach identified functional cis-regulatory regions, we generated
212 transcriptional reporter constructs expressing nuclear localized GFP under the control of the
213 guard cell specific ACRs upstream of the malate-transporter encoding gene *ALMT6* (54) and the
214 wax biosynthesis enzyme-encoding gene *AAE9* (55). Both reporter constructs produced guard
215 cell specific GFP signal in transgenic *Arabidopsis* leaves (Fig. 2I). In summary, we have
216 developed a robust protocol for isolating pure populations of guard cell nuclei allowing us to
217 discover cis-regulatory regions that are active in mature guard cells.
218
219 **ABA induces persistent chromatin remodeling in guard cells during stomatal closure**
220 We next asked whether epigenomic reprogramming occurs during ABA-induced stomatal
221 closure. Soil grown 6-week-old plants were sprayed with 50 uM ABA or control solution. After 3
222 hours, we confirmed a stomatal response by infrared photography (Fig. 3A). To determine if our
223 ABA treatment led to significant transcriptional changes we performed RNA-sequencing on both
224 whole leaf samples (Fig. S5A) and guard cell enriched samples (Fig. 3B). We observed that
225 ABA triggered the differential expression of thousands of transcripts in both whole leaves and
226 guard cells (2142 upregulated and 1574 downregulated in guard cells). As expected, ABA-
227 induced genes are enriched for the pathways “response to water deprivation” (p_value = 1.7e-
228 22), “response to abscisic acid” (pvalue = 4.47e-18), and “response to salt stress (Fig. S5D).
229 Although most of the transcriptional changes induced by ABA were shared between guard cells
230 and whole leaves, we found that 22.7% (488) of ABA-induced transcripts and 42.7% (673) of
231 ABA-repressed transcripts were specific to guard cells (Fig. S5C, Dataset S5). For instance,
232 ABA-regulated expression of the major facilitator protein-encoding gene *AT2G37900* and the
233 gene *AAE9* was only evident in guard cells (Fig. S5E).

234

235 To evaluate if ABA changed chromatin accessibility and whether these changes are sustained
236 over time following a single treatment, we isolated guard cell nuclei at 4 hours and 24 hours
237 after spraying (Fig. 3A). We generated ATAC-seq libraries from three biological replicates per
238 time point. PCA analysis showed that samples clustered together according to treatment (Fig.
239 S6A). Differential chromatin accessibility analysis found that ABA extensively reshapes
240 chromatin structure in guard cells with 2323 ACRs gaining accessibility and 1657 ACRs losing
241 accessibility across the treatment time course (Fig. 3C, Fig. S7A and B, and Dataset S3). We
242 next analyzed the temporal characteristics of this response by comparing the ATAC-seq
243 datasets from the 4-hour and 24-hour timepoints. Our results allowed us to define three
244 categories of ABA-regulated ACRs – early, sustained, and late (Fig. 3D). Strikingly, we found
245 that 1093 of the 2079 (52.6%) ACRs opened by ABA at 4 hours remained open after 24 hours.
246 Of the 975 ACRs closed by ABA at 4 hours 594 (61%) remained closed at 24 hours.
247 Additionally, we found 230 ACRs gained and 682 ACRs lost accessibility only 24 hours after
248 ABA treatment (Fig. 3D). Interestingly, we found differences in downstream gene GO term
249 enrichment between early and late ACRs. For example, the terms “response to light” and
250 “defense response” were strongly enriched in ABA-repressed ACRs only at 24 hours after ABA
251 treatment (Table S6).

252

253 Consistent with our observations in seedling roots (Fig. 1D), we found that ABA-regulated
254 ATAC-seq peaks in guard cells reside further away from transcription start sites (TSS) than non-
255 regulated peaks (> 1kb), indicating that distal regulation may be a characteristic of ABA-
256 controlled CREs (Fig. S6B). ABA-induced ACRs in guard cells are clearly associated with
257 downstream genes that are upregulated transcriptionally by ABA, while ABA-repressed ACRs
258 are associated with genes downregulated by ABA (Fig. 3E). Indeed, ABA-induced changes in
259 chromatin accessibility were correlated with ABA-induced differential expression of downstream

genes (r = 56, Fig. S6C). Examination of individual genes like the ABA-upregulated *MYB121* and the ABA-downregulated *MYB60* (56) illustrate the connection between upstream chromatin accessibility and transcript levels (Fig. 3F). Interestingly, we found that ABA modifies chromatin accessibility upstream of many known regulators of stomatal conductance including *KAT1*, *NCED3*, and *HT1* (57) as well as many other genes with no known stomatal functions (Fig. S6D-K, Table S3).

We next performed TF binding motif analysis on early, sustained, and late ABA-regulated ACRs using a set of DAP-seq derived motifs (43) restricted to those TFs with guard cell expression in our RNA-seq datasets. Both early and sustained ABA-induced ACRs had strong enrichment for motifs recognized by ABRE- binding TFs including ABI5, ABF1,2, and 3 (Fig. 3G). Interestingly, we found that the motifs recognized by CBF2, CBF3, and MYB61 (58–60) were preferentially enriched in early ABA-induced ACRs. ABA-repressed ACRs showed strong enrichment for motifs recognized by a clade of related bHLH-type TFs (Fig. S6L) including AKS1, AKS3, and bHLH80 in both sustained and late categories (Fig. 3H). In contrast, MYB96 motifs were enriched only in late appearing ABA-repressed ACRs (Fig. 3H). Collectively, our results demonstrate that ABA can induce persistent changes to chromatin in guard cells and expose the temporal regulation of different TFs during this response.

By analyzing published genome-wide DAP-seq datasets (39, *56*) we found strong ABF2 DAP-seq signal coincident with ABA-induced ACRs in guard cells (Fig. 3C). DAP-seq signals for ABF1, ABF3, and ABF4 were also enriched over regions that gain accessibility in response to ABA, although to a lesser extent than ABF2 (Fig. S6M). In contrast, ABA-repressed ACRs contained AKS1 DAP-seq binding sites (Fig. 3C). Additionally, unbiased de novo motif discovery (62) returned motifs similar to ABF1 and AKS3 binding sites as the most enriched in ABA-activated and ABA-repressed ACRs, respectively (p = 1e-119 and p = 1e-57). Metaplots of

ATAC-seq signal centered over peaks containing these motifs further supported our observation that ABA elevates chromatin accessibility at ABF binding sites and represses chromatin accessibility at AKS binding sites (Fig. S6N). Interestingly, ABA closed chromatin upstream of *AKS3* and decreased *AKS3* transcript levels in guard cells (Fig. 3I). We also observed that GFP-AKS3 signal decreased in ABA-treated guard cells when expressed from its native promoter (Fig. 3J).

Furthermore, by comparing ABA-induced ACRs from guard cells, mesophyll cells (Fig. S3E-G), and root cells (Fig. 1) we uncovered significant tissue/cell-type specificity in this response (Fig. 3K, Fig S7C-L). Interesting, we found that ABA had a much larger impact on chromatin accessibility in guard cells than in the other cell types with more ABA regulated regions (2079 ACRs compared with 1293 in roots and 926 in mesophyll) and larger fold changes in accessibility (Dataset S3). In conclusion, we show that ABA drives large scale changes to chromatin structure in guard cells and implicate major roles for the activation of ABFs and inhibition of AKSs in this response.

ABF transcription factors are required for ABA-induced chromatin opening in guard cells

The mechanisms that cause ABA-specific chromatin opening are unknown. Given the strong enrichment of ABF binding motifs in ABA-activated ACRs, and their coincidence with ABF *in vitro* binding sites, we wondered if these TFs might be required for reshaping chromatin during ABA-induced stomatal closure. To test this, we used the *abf1/2/3/4* (*abfx4*) quadruple mutant which lacks four related ABF proteins that are prominent during vegetative growth (25, 26). We first performed RNA-seq following ABA treatment on leaves from 6-week-old *abf1/2/3/4* (*abfx4*) mutant plants (Fig. S8A). Of the 2469 transcripts that are upregulated by ABA in wild type leaves, 2030 (~82%) depend on ABF1/2/3/4 (Fig. S8B). Interestingly, although ABA increased *ABF1/2/3/4* transcript levels in guard cells we did not find that ABA altered chromatin

accessibility in the upstream regions near the corresponding genes (Fig. S8C). We conclude that ABF1/2/3/4 are required for the bulk of ABA-induced gene expression in mature leaf tissue. Plants lacking *ABF1/2/3/4* (*abfx4*) are highly sensitive to drought stress and lose water faster than wild type plants in detached leaf assays (26). Consistent with this, we observed that *abfx4* mutant plants exhibited higher steady-state stomatal conductances than *Col-0* control plants (Fig. S8D).

Under non-stressed conditions, guard cells have a higher ABA concentration than other leaf cell types (42, 63). Recent studies have provided evidence for basal ABA signaling in guard cells and defined important roles for basal ABA in stomatal function (64, 65). By generating guard cell FANS lines in an *abfx4* mutant background (Fig. S9A) we were able to assess the impact of the loss of ABF1/2/3/4 on guard cell chromatin in non-stressed plants. In the absence of ABA treatment, we observed minimal differences in genome-wide patterns of chromatin accessibility between WT and abfx4 guard cells (Fig S9B, C and Dataset S3) suggesting that basal ABA signaling in guard cells may regulate mainly post-transcriptional stomatal closing mechanisms, but does not significantly regulate chromatin structure.

Next, we asked if the ABF1/2/3/4 are required for the ability of ABA to reshape chromatin structure. Strikingly, loss of *abf1/2/3/4* strongly impaired ABA-induced chromatin opening in guard cells but had less impact on ABA-triggered chromatin closing (Fig. 4A, Dataset S7). Of the 2079 ABA-induced ACRs, 1539 (~74%) required ABF1/2/3/4 for gained accessibility (Fig. 4B). ABF-dependent ABA-induced ACRs were strongly enriched for ABREs (example ABF1, p = 1e-86), while ABF-independent ABA-induced ACRs were most strongly enriched for CBF1/2/3 motifs (example CBF1, p = 1e-16) (Dataset S7). Examination of individual loci like the ABA-activated genes *DTX37* and *HSFA6B* revealed a close connection between abf-dependent increases in upstream chromatin accessibility and abf-dependent transcription (Fig. 4C).

We next performed TF motif analysis on ABA-regulated accessible chromatin regions in both *WT* and *abfx4* mutant guard cells. As expected, *abfx4* mutants were depleted for ABRE motif enrichment in ABA-induced ACRs but notably retained enrichment for AKS1, AKS3, and bHLH80 motifs in ABA-repressed ACRs (Fig. 4D, Dataset S7). Additionally, although most TF binding sites lost enrichment in ABA-induced ACRs in the absence of ABF1/2/3/4, we found that enrichment for motifs bound by CBF1/2/3 was preserved. TF binding motifs are often information poor and the presence of a motif at a genomic location does not always lead to TF action. Analysis of published ABF1/2/3/4 binding assays conducted on naked genomic DNA (61) uncovered 11334 binding sites, but only 1315 resided within ABA-induced ACRs in guard cells (Fig. 4E). However, ABA-induced chromatin opening at these ACRs containing ABF-binding sites was strongly impaired in *abfx4* mutant guard cells (Fig. 4F). We reasoned that chromatin structure may determine which *in vitro* ABF binding sites are functional. To test this idea, we examined if ABF DAP-seq peaks found within ABA-induced ACRs could predict ABA-activated transcription. Using our guard cell RNA-seq data, we found that ABF binding sites that reside within regions of ABA regulated open chromatin were more strongly associated with downstream ABA-induced genes than were an equal number of random ABF-binding sites (Fig. 4G).

To examine the temporal characteristics of ABF-dependent chromatin remodeling we focused on roots where ABA can reshape chromatin by 45 mins (Fig. 1C). We performed ATAC-seq on isolated *abfx4* mutant root nuclei over an ABA treatment time course and found that ABA fails to drive progressive chromatin opening in this background (Fig. S10). In *abfx4* mutant roots, 45 mins of ABA treatment induced only 2 ACRs compared to 163 in wild type roots. By 2 hours of ABA treatment, only 27 ABA-induced ACRs were present in *abfx4* mutants compared with 601 in wild type (Fig. 4H , Fig. S10A, and Dataset S3). However, ABA repressed a similar number of

364 root ACRs in the absence of ABF1/2/3/4 (Fig. 4H and Fig. S10A). Although our data support a
365 general requirement for ABFs in ABA-induced chromatin opening in roots and guard cells, we
366 do find that some guard cell specific ABA-induced ACRs are ABF-dependent (Fig. S10D,E).
367 Collectively, these results demonstrate that the ABF1/2/3/4 transcription factors are required for
368 triggering genome-wide chromatin opening in response to ABA.
369

370 **ABA and changes to atmospheric CO_2 concentration induce distinct chromatin**
371 **remodeling programs in guard cells**

372 Because we observed that ABA has extensive effects on chromatin accessibility in guard cells,
373 we wondered whether chromatin structure may respond to other stimuli that drive stomatal
374 movements. Here we focus on changes to atmospheric CO_2 concentration. Exposure of plants
375 to low CO_2 stimulates stomatal opening while high CO_2 drives stomatal closure (Fig 5A). The
376 exact role of ABA signaling during CO_2 induced stomatal responses is unclear and is a matter of
377 some debate (64–66). Recent studies suggest that although high-CO_2 induced stomatal closure
378 requires basal ABA signaling it does not involve further SnRK2 kinase activation (64, 65).
379 Comparing how these signals impact genome activity could provide new insight into whether
380 and how the mechanisms underlying guard cell responses to ABA and CO_2 may differ.
381

382 To generate low and high CO_2 guard cell ATAC-seq libraries we exposed 6-week-old plants to
383 either 100 ppm CO_2 or 1000 ppm CO_2 for 4 hrs, two treatments that induce robust stomatal
384 responses (Fig 5B). Surprisingly, in contrast to the extensive effect of ABA on chromatin
385 accessibility in guard cells (Fig. 5C), we observed smaller changes in response to low CO_2 (Fig.
386 5D), and minimal changes following treatment with high CO_2 (Fig. 5E). Following exposure of
387 plants to 100 ppm CO_2, 329 ACRs gained accessibility and 487 ACRs lost accessibility while
388 treatment with 1000 ppm CO_2 induced only 11 ACRs and repressed 79 ACRs (Dataset S3).
389 Heatmaps of ATAC-seq signal at ABA and Low CO_2-regulated regions highlighted the specificity

390 of these responses (Fig. 5F, Fig. S7A,B). PCA results comparing our guard cell ATAC-seq
391 datasets from different conditions further support these findings and revealed little difference
392 between control and high CO_2 treatments (Fig. 5G). Examination of individual loci highlights the
393 specificity of these responses, for instance chromatin opening upstream of *ERF113* only
394 occurred in response to ABA while the upstream region of the PP2C-encoding *AT2G25070*
395 gains accessibility only in response to low CO_2 (Fig. S11B-E).
396
397 Analysis of the set relationships among ABA, low CO_2, and high CO_2 regulated ACRs revealed
398 little overlap suggesting that these stimuli control distinct cis-regulatory elements in the genome
399 (Fig. S11A). We did find significant overlap between ABA-induced and low CO_2-repressed
400 ACRs and between ABA-repressed and low CO_2-induced ACRs. ABA-repressed regions had
401 elevated average ATAC-seq signal in guard cells isolated from plants exposed to 100 ppm
402 [CO_2] (Fig. 5F). For instance, ABA-repressed chromatin accessibility upstream of *ALMT6* while
403 low-CO_2 treatment enhanced accessibility (Fig. S11D). Interestingly, ABA repressed chromatin
404 accessibility upstream of *HT1*, *BLUS1*, and *CBC2* (67), all key positive regulators of low CO_2-
405 and blue light-induced stomatal opening, while high CO_2 had no effect (Fig. 5H). These data
406 indicate that chromatin remodeling represents an important cross talk point for these stimuli,
407 ensuring robust stomatal closing or opening, depending on the physiological conditions. DNA
408 binding motif analysis further emphasized the distinct regulatory impacts of changes in CO_2
409 concentration and ABA on the genome (Table S7). In contrast with ABA-induced ACRs, we did
410 not find enrichment of ABF binding motifs in low or high CO_2 regulated chromatin (Fig. 5I).
411 Instead, low CO_2 gained ACRs were enriched for motifs recognized by C2C2dof-type TFs which
412 were oppositely enriched only in ABA-repressed ACRs. Collectively, our data demonstrate how
413 different signals that control stomatal movement deploy distinct gene regulatory programs in
414 guard cells.
415

DISCUSSION

Abscisic acid triggers changes in gene expression, but whether this transcriptional response depends on chromatin remodeling remained unknown (5). Here, we reveal massive ABA-induced chromatin remodeling pointing to an orchestrated reprogramming of the *Arabidopsis* epigenome by specific sets of transcription factors. We identify regulatory regions of the genome specifically active in guard cells and uncover how the accessibility of these sequences is modified by signals that control stomatal aperture size.

Guard cell regulation of stomatal aperture size is essential for plant survival under drought stress. Such regulation requires that the guard cells forming the stomatal pore integrate numerous physiological and environmental cues. In this study, we profiled genome-wide chromatin accessibility in tens of thousands of guard cells isolated from soil-grown plants exposed to different stimuli that trigger stomatal movements. Our results lead us to propose that guard cell ABA signaling controls the balance between two opposing chromatin states. Under unstressed conditions, AKS proteins maintain open chromatin at upstream regulatory regions of ABA-repressed genes while ABA-activated genes are kept silent by closed chromatin. Under abiotic stress such as drought, ABA levels rise in guard cells thereby activating SnRK2 kinases which subsequently inhibit AKSs and activate ABFs. This leads to chromatin opening upstream of abiotic stress-activated genes and the loss of chromatin accessibility upstream of stress-repressed genes.

We uncovered patterns of chromatin accessibility specific to guard cells (Fig. 2D) and identified cis-regulatory regions supporting guard cell specific gene expression (Fig. 2F-I and Dataset S4). We found that ABA induces extensive and cell-type specific chromatin remodeling and that guard cells possess a more extensive response than mesophyll and root cells (Fig. 3K and Fig.

S7C-L). Importantly, we find that these ABA-induced chromatin remodeling events correlate with ABA-regulated gene expression (Fig. 3E and S6C). By performing TF-binding motif enrichment and analyzing published DAP-seq data, we hypothesized that the bZIP transcription factors ABF1/2/3/4 may function in ABA-induced chromatin remodeling in guard cells (Fig. 3C,G and Fig. S6M). Interestingly, we find that among *in vitro* ABF binding sites, those occurring within ABA-opened chromatin are most strongly associated with ABA-induced transcription (Fig. 4G), indicating that regulated chromatin accessibility may determine which genomic ABF binding sites are functional. Our experiments in *abf1/2/3/4* quadruple mutant guard cells demonstrate that these four transcription factors are essential for the majority of ABA-triggered chromatin opening (Fig. 4). Furthermore, experiments in root nuclei show that in *abf1/2/3/4* quadruple mutants, even early ABA-induced chromatin remodeling events are strongly impaired (Fig. 4H and Fig. S10), suggesting that ABFs initiate chromatin opening. How ABFs accomplish chromatin opening remains to be determined, but existing literature could be interpreted to support two possible and not necessarily mutually exclusive explanations. (1) Although nucleosomes can restrict TF binding to DNA, some TFs, known as pioneer factors (68, 69), possess the ability to bind their target sequences even within inaccessible chromatin regions. At present, only a handful of pioneer factors have been documented in plants (70). While our data are consistent with ABFs acting as pioneer factors, future biochemical experiments reconstituting ABF binding to nucleosomal DNA are needed to investigate this model. (2) ABFs may recruit chromatin modifying proteins to target sequences which could increase chromatin accessibility. Interestingly, several such molecules including the SWI/SNF ATPase BRM (71, 72) and the histone deacetylase HDA9 (73) interact with known ABA signaling components. Furthermore, ABF-binding proteins known as AFPs, which negatively regulate ABA signaling, have been shown to physically interact with histone and chromatin modifying factors (74).

467 Although our data support a general requirement for ABF proteins in both roots and guard cells,
468 we also observe that ABA alters chromatin accessibility in a cell-type specific manner. At
469 present we do not understand how ABFs might contribute to cell-type specific regulation of
470 chromatin. Beyond ABF1/2/3/4, our analyses implicated additional TFs in ABA-dependent
471 genome reprogramming (Fig. 3F and 3G), which is consistent with prior research showing that
472 ABA regulates the binding of multiple transcription factors (75). We observed that ~26% of ABA-
473 gained ACRs (540 ACRs) still open in *abfx4* mutant guard cells in response to ABA (Fig. 4B).
474 These ABF-independent regions retained enrichment for CBF1/2/3 binding motifs, suggesting
475 that CBF transcription factors display ABF-independent binding (Fig. 4D). Finally, although ABA-
476 induced chromatin opening is severely impaired in *abf1/2/3/4* quadruple mutant guard cells, we
477 cannot exclude the possibility that other ABRE-binding TFs, in particular ABI5 (76, 77),
478 participate in this process as well.
479
480 Notably, our data suggest that the related bHLH transcription factors AKS1/2/3 play a larger role
481 in the regulation of ABA-repressed genes than was previously thought. Prior research had
482 shown that SnRK2 kinase-dependent inhibition of AKS1/2 was required for the ABA-dependent
483 transcriptional repression of the K+ ion channel gene *KAT1* in guard cells (24). Surprisingly, we
484 found that AKS1 bound many regions in the genome that lose chromatin accessibility in guard
485 cells following ABA treatment (Fig. 3C). Additionally, motifs recognized by AKS1/3 and the
486 related protein bHLH80 were enriched in ABA-repressed ACRs in guard cells (Fig. 3H), as well
487 as in root and mesophyll cells (Fig. 1F, Fig. S3G, Table S7). This observation was further
488 supported by de novo motif analysis (Fig S6N). AKS1 and AKS2 are inhibited by direct ABA-
489 dependent SnRK2 phosphorylation, but their expression was not controlled by ABA signaling
490 (44). We found that in guard cells, ABA represses *AKS3* expression implying that ABA-
491 dependent inhibition of AKS proteins occurs through both transcriptional and phosphorylation-
492 dependent mechanisms (Fig. 3I and J).

493

494 Elevation in the CO_2 concentration in leaves triggers rapid stomatal closing (34). The extent to
495 which elevated atmospheric CO_2 signals through the ABA signal transduction pathway is
496 currently under debate. Different research groups using the same mutants have come to
497 different conclusions regarding direct CO_2 signaling via the early ABA receptor/SnRK2 kinase
498 pathway during CO_2-induced stomatal closure. Our results exposed major differences in how
499 guard cells interpret these stimuli. In contrast to the extensive and persistent changes to
500 chromatin structure induced by ABA (Fig. 3), exposure to elevated CO_2 had minimal impact on
501 genome-wide chromatin accessibility in guard cells (Fig. 5). While ABA controlled chromatin
502 accessibility at 3018 ACRs in the genome, we found that only 90 ACRs were regulated by
503 elevated CO_2 (Fig 5C-E). Additionally, the strong enrichments of ABF binding motifs in gained
504 ACRs and AKS binding motifs in lost ACRs, evident following ABA treatment, are absent during
505 the response to elevated CO_2 (Fig. 5I). The disparity between these two signals at the level of
506 chromatin mirrors the disparity between characteristics of their respective physiological
507 responses. Unlike ABA- and drought-triggered stomatal closure, elevated CO_2-induced stomatal
508 closure is rapidly reversed upon return to ambient CO_2 (64). Such rapid changes in the
509 intercellular CO_2 concentration in leaves occur for example with alternating light intensities (e.g.
510 passing cloud cover) and require rapid reversals of stomatal CO_2 responses. Furthermore, we
511 found that exposure to low CO_2 triggers a distinct program of chromatin remodeling in guard
512 cells (Fig. 5F-I).

513

514 Finally, our results may open new avenues for investigation into two poorly understood features
515 of stomatal biology. Studies in multiple plant species have documented a phenomenon referred
516 to as stomatal “memory” (78, 79). Following drought stress and re-watering, plants typically
517 exhibit delayed and/or slow re-opening of stomata despite rapid recovery of plant water status.
518 Furthermore, guard cells display transcriptional memory where repetitive dehydration stress

leads to altered transcript levels in subsequent stress events (80–82). We found that ABA triggered changes to chromatin accessibility in guard cells that can persist for up to 24 hours, which could prime the genome for subsequent abiotic stress exposure (Fig. 3). These shifts occurred at thousands of locations in the genome including upstream of many genes known to regulate stomatal movements as well as many genes with potential functions in stomatal physiology that could be the basis for future studies (Fig. S6 and Dataset S3). Moreover, our findings support crosstalk between ABA and low CO_2 signaling at the chromatin remodeling level. For example, we uncovered that ABA, but not high CO_2, triggered chromatin closing upstream of genes encoding key CO_2-sensing and signaling proteins that promote low CO_2-induced stomatal opening, including *HT1*, *BLUS1*, and *CBC2* (Fig. 5H). This response may contribute to the long-term stomatal closing triggered by drought and ABA by inhibiting mechanisms for low CO_2-induced stomatal opening. ABA-triggered chromatin dynamics may provide a basis for long-term reprogramming of the guard cell genome for abiotic stress survival. We envision that these sustained changes to chromatin structure may store the experience of drought stress and contribute to long-term adjustments of stomatal function.

METHODS

Plant material and growth conditions

The Columbia-0 (Col-0) accession of *Arabidopsis thaliana* was used as the wild-type background. Experiments on seedlings were conducted using plants germinated and grown on 1/2 Murashige and Skoog (MS) media (pH 5.7-8) solidified with 1% Phyto-agar plates. Experiments using mature plants were conducted using plants grown in soil (Sunshine Mix #1) filled plastic pots incubated in a growth chamber (Conviron) under a 12hr-12hr light-dark cycle, a light intensity of 100 µmol m^{-2} s^{-1}, a temperature of 22 C, ambient [CO_2], and a relative humidity of 65%. To minimize the impact of environmental variation all experiments were performed on plants grown in two identical growth chambers equipped with [CO_2] control.

ABA treatments in plate-based experiments were performed using a mesh (100 µm polyester) transfer method. Seeds were germinated on ½ MS agar plates overlaid with sterilized polyester mesh (100 µm). ABA treatments were initiated by transferring 8-day-old seedlings in mass to plates containing 50 µM ABA (Sigma cis/trans-abscisic acid) or to plates containing vehicle control (Ethanol). ABA treatments on soil grown plants were performed by spraying plants with 50 µM ABA diluted with 0.01% Silwet (in water) or with vehicle control. To assess treatment responses, leaf temperature was measured using an infrared thermal imaging camera (T650sc; FLIR).

Plasmid DNA and plant transformation

Constructs for cell-type specific nuclear sorting were prepared using multi-site gateway technology (Invitrogen). The ORF encoding the histone H2B (*AT5G22880*) was cloned in a pDONR221 entry vector. The cell type specific promotors RBCp and GC1p, from the Rubisco small subunit 2B gene (*AT5G38420)* and the *GASA9* (*AT1G22690*) gene respectively, were cloned from the *Arabidopsis* genome into the gateway entry vector pDONR-p4p1r. Final plant transformation constructs were generated by performing multisite gateway recombination into the pP7m34GW destination vector. The plasmid for expressing *GFP-AKS3* under the *AKS3* (*AT2G42280*) endogenous promotor was generated using GreenGate cloning (83). The cloned *AKS3* upstream regulatory sequence was defined using guard cell ATAC-seq data. Transcriptional reporter constructs expressing nuclear localized GFP under the guard cell specific ACRs upstream of *AAE9* (*AT1G21540*) and *ALMT6* (*AT2G17470*) were generated using GreenGate cloning. Primer sequences are available in Dataset S8. Constructs were transformed into *A. thaliana* Col-0 plants using the floral dipping technique with *Agrobacterium tumefaciens* strain GV3101.

571 **Microscopy**

572 Plant leaves were mounted on conventional glass microscope slides in water with the abaxial
573 epidermal layer against the coverslip. GFP and chlorophyll fluorescence signals were recorded
574 using either an Eclipse TE2000-U (Nikon, Tokyo, Japan) spinning disc confocal microscope or a
575 Leica SP8 confocal microscope (Leica Microsystems). Constant gain, laser power, and
576 exposure times were used for each experiment when comparing treatments/samples. On the
577 Leica SP8 images were acquired using a 512 x 512 pixel resolution and a scan speed of 400
578 Hz. Displayed images are representative of at least 4 different leaves harvested from two
579 independent transgenic lines. Images were processed for publication using Fiji software. 3D
580 reconstructions from confocal imaging data were generated using Leica LAS X Software.

581

582 **Time resolved stomatal conductance measurements**

583 For gas exchange experiments, *Col-0* and *abfx4* mutant plants were grown together in the same
584 growth chamber to minimize biological variation. Intact leaves of six-week-old plants were used
585 for gas exchange experiments. Stomatal conductance was measured using a Licor-6400
586 infrared gas exchange analyzer equipped with a leaf chamber (LI-COR Biosciences). Before
587 beginning measurements, clamped leaves were equilibrated for 45-60 mins at 150 µmol m^{-2} s^{-1}
588 light intensity, ~65% relative humidity, 21ºC, 400 ppm [CO_2], and an air flow of 400 µmol s^{-1}.
589 Stomatal conductance was recorded every 30 seconds for a total of 30 min. To control for the
590 effect of the diurnal rhythm on stomatal physiology, gas exchange experiments began 2 hr after
591 the beginning of the light cycle and measurements were made alternating between different
592 genotypes. Data are presented as average stomatal conductance +/- standard error of 5 plants
593 per genotype.

594

595

596

597 **Fluorescence-activated nuclear sorting (FANS)**

598 FANS on seedling/root nuclei and mesophyll nuclei was performed similar to (40) with small
599 modifications. Briefly, whole seedlings, surgically isolated roots, or leaves were chopped
600 vigorously with a clean razor blade in 2-3 ml of ice-cold FANS-lysis buffer (15 mM Tris-HCl
601 pH7.5, 20 mM NaCl, 80 mM KCl, 0.2 mM spermine, 5 mM 2-ME, 0.5 mM spermidine, 0.2%
602 IGEPAL CA-630, Roche mini EDTA-free Protease Inhibitor Cocktail) for 5 minutes in a cold
603 glass petri dish. The subsequent lysate was filtered through a 40 µm filter unit before
604 transferring to a 15 ml tube containing 3 ml of FANS-Sucrose buffer (20 mM Tris-HCl pH 8.0, 2
605 mM $MgCl_2$, 2 mM EDTA, 15 mM 2-ME, 1.7 M sucrose, 0.2% IGEPAL CA-630). Nuclei were
606 pelleted at 2500xG at 4ºC for 25 mins, after which the supernatant was carefully removed. The
607 nuclei pellet was then gently resuspended, using clipped pipette tips, with 600 µl FANS-lysis
608 buffer supplemented with DAPI, and then immediately used for flow cytometry.
609 For experiments on guard cells, the leaves of ~40 six-week-old plants were harvested and
610 blended in 500 ml of ice-cold water for 2x40 secs with 1 min between pulses. The blended
611 sample was then poured over a 100 µm mesh to remove mesophyll cells and collect epidermal
612 enriched fragments. The mesh was gently rinsed with ~200 ml of cold water and gently blotted
613 with paper towels to remove excess liquid. Thin sections of the collected epidermal tissue were
614 then flash-frozen in liquid nitrogen. Epidermal sections were ground to a fine powder with a
615 frozen mortar and pestle. After grinding, powder was transferred to a new mortar with a frozen
616 metal spatula. Immediately 12-15 ml of ice-cold FANS-lysis buffer was added, and the powder
617 was gently resuspended with a clean pestle. The subsequent lysate was filtered through a 40
618 µm filter unit before transferring to a 15 ml tube containing 6 ml of FANS-Sucrose buffer. Nuclei
619 were then pelleted and prepared for FACS as above.
620
621 Flow cytometry was conducted on a BD FACS Aria II using a 70 µm nozzle with a flow rate < 2
622 and the following photomultiplier parameters: Forward Scatter (FSC) – 250 eV, Side Scatter

(SSC) – 220 eV, BV421 (DAPI channel) – 550 eV, FITC (GFP channel) – 340 eV. Sort gates were defined empirically using the FSC and SSC channels to exclude debris and potential doublets. Before sorting GFP labeled nuclei, FACS analysis on unlabeled control samples (Col-0 nuclei) was performed to define background fluorescence signal. When isolating guard cell nuclei, sort gates were established to purify exclusively 2N (diploid) and GFP-positive nuclei. To evaluate the purity of sorted samples, a fraction (~10% of total volume) was re-run under the same sorting program (e.g. Fig. S2D). Sorted nuclei were collected in 600 µl of FANS-lysis buffer in a refrigerated tube chamber. After sorting, nuclei were pelleted by centrifugation at 1000xg for 10 mins at 4C. Nuclei pellets were gently washed with 1 ml of 10 mM Tris-HCl pH 8.0, 5 mM MgCl2 buffer, before centrifugation again as above. After carefully removing the supernatant, nuclei were used immediately for ATAC-seq.

Detailed protocols for RNA-seq and ATAC-seq library preparation and description of ATAC-seq, RNA-seq, and DAP-seq data analyses can be found in the SI Appendix, Materials and Methods.

Competing interest statement

The authors declare no competing interests.

Acknowledgements

Funding for this study was provided by the National Institutes of Health (R01GM060396 to J.I.S and F32GM137544 to C.A.S). CO_2 experiments were supported by National Science Foundation grant MCB-1900567 to J.I.S. This study includes data generated at the UC San Diego IGM Genomics Center utilizing an Illumina NovaSeq 6000 that was purchased with funding from a National Institutes of Health SIG grant (#S10 OD026929). Microscopy was supported by the UC San Diego Microscopy Core with funding by grant NINDS P30NS047101. We thank Kazuko Yamaguchi-Shinozaki (University of Tokyo) for sharing *abf1/2/3/4* quadruple

mutant seeds, and members of the Schroeder lab for helpful discussions throughout the research.

Author contributions: C.A.S. and J.I.S. conceived of the study and designed the methodology. C.A.S. performed all experiments and analyzed the data. C.A.S. and J.I.S. wrote and edited the paper.

Data and materials availability: All materials (plasmids, seed stocks) are available upon request. Raw FASTQ files generated in this study are available upon publication at NCBI's Sequence Read Archive. All data are available in the main text and supplementary material.

REFERENCES

1. R. J. Schmitz, E. Grotewold, M. Stam, Cis-regulatory sequences in plants: Their importance, discovery, and future challenges. *The Plant Cell* **34**, 718–741 (2022).

2. W. K. M. Lai, B. F. Pugh, Understanding nucleosome dynamics and their links to gene expression and DNA replication. *Nature Reviews Molecular Cell Biology* **18**, 548–562 (2017).

3. T. C. Voss, G. L. Hager, Dynamic regulation of transcriptional states by chromatin and transcription factors. *Nature Reviews Genetics* **15**, 69–81 (2014).

4. J. L. Nemhauser, F. Hong, J. Chory, Different Plant Hormones Regulate Similar Processes through Largely Nonoverlapping Transcriptional Responses. *Cell* **126**, 467–475 (2006).

5. R. Waadt, *et al.*, Plant hormone regulation of abiotic stress responses. *Nat Rev Mol Cell Biol* **23**, 680–694 (2022).

6. P. Sijacic, M. Bajic, E. C. McKinney, R. B. Meagher, R. B. Deal, Changes in chromatin accessibility between Arabidopsis stem cells and mesophyll cells illuminate cell type-specific transcription factor networks. *The Plant Journal* **94**, 215–231 (2018).

7. K. A. Maher, *et al.*, Profiling of Accessible Chromatin Regions across Multiple Plant Species and Cell Types Reveals Common Gene Regulatory Principles and New Control Modules. *The Plant Cell* **30**, 15–36 (2018).

8. A. M. Sullivan, *et al.*, Mapping and Dynamics of Regulatory DNA in Maturing Arabidopsis thaliana Siliques. *Frontiers in Plant Science* **10** (2019).

9. A. Farmer, S. Thibivilliers, K. H. Ryu, J. Schiefelbein, M. Libault, Single-nucleus RNA and ATAC sequencing reveals the impact of chromatin accessibility on gene expression in Arabidopsis roots at the single-cell level. *Molecular Plant* **14**, 372–383 (2021).

10. M. Borg, *et al.*, Epigenetic reprogramming rewires transcription during the alternation of generations in Arabidopsis. *eLife* **10**, e61894 (2021).

11. A. P. Marand, Z. Chen, A. Gallavotti, R. J. Schmitz, A cis-regulatory atlas in maize at single-cell resolution. *Cell* **184**, 3041-3055.e21 (2021).

12. E.-D. Kim, *et al.*, Dynamic chromatin accessibility deploys heterotypic cis/trans-acting factors driving stomatal cell-fate commitment. *Nat. Plants* **8**, 1453–1466 (2022).

13. K. C. Potter, J. Wang, G. E. Schaller, J. J. Kieber, Cytokinin modulates context-dependent chromatin accessibility through the type-B response regulators. *Nat. Plants* **4**, 1102–1111 (2018).

14. M. A. Reynoso, *et al.*, Evolutionary flexibility in flooding response circuitry in angiosperms. *Science* **365**, 1291–1295 (2019).

15. E. S. Karaaslan, N. Faiß, C. Liu, K. W. Berendzen, Isolation of Lineage Specific Nuclei Based on Distinct Endoreduplication Levels and Tissue-Specific Markers to Study Chromatin Accessibility Landscapes. *Plants* **9**, 1478 (2020).

16. S. R. Cutler, P. L. Rodriguez, R. R. Finkelstein, S. R. Abrams, Abscisic Acid: Emergence of a Core Signaling Network. *Annual Review of Plant Biology* **61**, 651–679 (2010).

17. R. Finkelstein, Abscisic Acid Synthesis and Response. *Arabidopsis Book* **11** (2013).

18. J.-K. Zhu, Abiotic Stress Signaling and Responses in Plants. *Cell* **167**, 313–324 (2016).

19. Y. Ma, *et al.*, Regulators of PP2C Phosphatase Activity Function as Abscisic Acid Sensors. *Science* **324**, 1064–1068 (2009).

20. S.-Y. Park, *et al.*, Abscisic Acid Inhibits Type 2C Protein Phosphatases via the PYR/PYL Family of START Proteins. *Science* **324**, 1068–1071 (2009).

21. T. Umezawa, *et al.*, Type 2C protein phosphatases directly regulate abscisic acid-activated protein kinases in Arabidopsis. *Proceedings of the National Academy of Sciences* **106**, 17588–17593 (2009).

22. H. Fujii, P. E. Verslues, J.-K. Zhu, Identification of Two Protein Kinases Required for Abscisic Acid Regulation of Seed Germination, Root Growth, and Gene Expression in Arabidopsis. *The Plant Cell* **19**, 485–494 (2007).

23. K. E. Hubbard, N. Nishimura, K. Hitomi, E. D. Getzoff, J. I. Schroeder, Early abscisic acid signal transduction mechanisms: newly discovered components and newly emerging questions. *Genes Dev.* **24**, 1695–1708 (2010).

24. Y. Takahashi, *et al.*, bHLH Transcription Factors That Facilitate K+ Uptake During Stomatal Opening Are Repressed by Abscisic Acid Through Phosphorylation. *Science Signaling* **6**, ra48–ra48 (2013).

25. T. Yoshida, *et al.*, AREB1, AREB2, and ABF3 are master transcription factors that cooperatively regulate ABRE-dependent ABA signaling involved in drought stress tolerance and require ABA for full activation. *The Plant Journal* **61**, 672–685 (2010).

26. T. Yoshida, *et al.*, Four Arabidopsis AREB/ABF transcription factors function predominantly in gene expression downstream of SnRK2 kinases in abscisic acid signalling in response to osmotic stress. *Plant, Cell & Environment* **38**, 35–49 (2015).

27. P. Wang, *et al.*, Quantitative phosphoproteomics identifies SnRK2 protein kinase substrates and reveals the effectors of abscisic acid action. *Proceedings of the National Academy of Sciences* **110**, 11205–11210 (2013).

28. T. Umezawa, *et al.*, Genetics and Phosphoproteomics Reveal a Protein Phosphorylation Network in the Abscisic Acid Signaling Pathway in Arabidopsis thaliana. *Sci. Signal.* **6**, rs8–rs8 (2013).

29. N. Leonhardt, *et al.*, Microarray Expression Analyses of Arabidopsis Guard Cells and Isolation of a Recessive Abscisic Acid Hypersensitive Protein Phosphatase 2C Mutant. *The Plant Cell* **16**, 596–615 (2004).

30. H. Goda, *et al.*, The AtGenExpress hormone and chemical treatment data set: experimental design, data evaluation, model data analysis and data access. *The Plant Journal* **55**, 526–542 (2008).

31. R.-S. Wang, *et al.*, Common and unique elements of the ABA-regulated transcriptome of Arabidopsis guard cells. *BMC Genomics* **12**, 216 (2011).

32. A. M. Hetherington, F. I. Woodward, The role of stomata in sensing and driving environmental change. *Nature* **424**, 901–908 (2003).

33. S. M. Assmann, T. Jegla, Guard cell sensory systems: recent insights on stomatal responses to light, abscisic acid, and CO2. *Current Opinion in Plant Biology* **33**, 157–167 (2016).

34. G. Dubeaux, *et al.*, Deep dive into CO2-dependent molecular mechanisms driving stomatal responses in plants. *Plant Physiology* **187**, 2032–2042 (2021).

35. Z. Liu, *et al.*, Global Dynamic Molecular Profiling of Stomatal Lineage Cell Development by Single-Cell RNA Sequencing. *Molecular Plant* **13**, 1178–1193 (2020).

36. C. B. Lopez-Anido, *et al.*, Single-cell resolution of lineage trajectories in the Arabidopsis stomatal lineage and developing leaf. *Developmental Cell* **56**, 1043-1055.e4 (2021).

37. J.-Y. Kim, *et al.*, Distinct identities of leaf phloem cells revealed by single cell transcriptomics. *The Plant Cell* **33**, 511–530 (2021).

38. C. Procko, *et al.*, Leaf cell-specific and single-cell transcriptional profiling reveals a role for the palisade layer in UV light protection. *The Plant Cell* **34**, 3261–3279 (2022).

39. J. D. Buenrostro, P. G. Giresi, L. C. Zaba, H. Y. Chang, W. J. Greenleaf, Transposition of native chromatin for fast and sensitive epigenomic profiling of open chromatin, DNA-binding proteins and nucleosome position. *Nature Methods* **10**, 1213–1218 (2013).

40. Z. Lu, B. T. Hofmeister, C. Vollmers, R. M. DuBois, R. J. Schmitz, Combining ATAC-seq with nuclei sorting for discovery of cis-regulatory regions in plant genomes. *Nucleic Acids Research* **45**, e41 (2017).

41. A. M. Jones, *et al.*, Abscisic acid dynamics in roots detected with genetically encoded FRET sensors. *eLife* **3**, e01741 (2014).

42. R. Waadt, *et al.*, FRET-based reporters for the direct visualization of abscisic acid concentration changes and distribution in Arabidopsis. *eLife* **3**, e01739 (2014).

43. R. C. O'Malley, *et al.*, Cistrome and Epicistrome Features Shape the Regulatory DNA Landscape. *Cell* **165**, 1280–1292 (2016).

44. Y. Takahashi, T. Kinoshita, M. Matsumoto, K. Shimazaki, Inhibition of the Arabidopsis bHLH transcription factor by monomerization through abscisic acid-induced phosphorylation. *The Plant Journal* **87**, 559–567 (2016).

45. Y. Yang, A. Costa, N. Leonhardt, R. S. Siegel, J. I. Schroeder, Isolation of a strong Arabidopsis guard cell promoter and its potential as a research tool. *Plant Methods* **4**, 6 (2008).

46. J. A. Anderson, S. S. Huprikar, L. V. Kochian, W. J. Lucas, R. F. Gaber, Functional expression of a probable Arabidopsis thaliana potassium channel in Saccharomyces cerevisiae. *Proceedings of the National Academy of Sciences* **89**, 3736–3740 (1992).

47. D. P. Schachtman, J. 1. Schroeder, W. J. Lucas, J. A. Anderson, R. F. Gaber, Expression of an Inward-Rectifying Potassium Channel by the Arabidopsis KAT1 cDNA. *Science* **258**, 1654–1658 (1992).

48. R. L. Nakamura, *et al.*, Expression of an Arabidopsis Potassium Channel Gene in Guard Cells. *Plant Physiology* **109**, 371–374 (1995).

49. O. S. Lau, *et al.*, Direct roles of SPEECHLESS in the specification of stomatal self-renewing cells. *Science* **345**, 1605–1609 (2014).

50. S.-K. Han, *et al.*, MUTE Directly Orchestrates Cell-State Switch and the Single Symmetric Division to Create Stomata. *Developmental Cell* **45**, 303-315.e5 (2018).

51. K. Ohashi-Ito, D. C. Bergmann, Arabidopsis FAMA Controls the Final Proliferation/Differentiation Switch during Stomatal Development. *The Plant Cell* **18**, 2493–2505 (2006).

52. H. Yu, *et al.*, Activated Expression of an Arabidopsis HD-START Protein Confers Drought Tolerance with Improved Root System and Reduced Stomatal Density. *The Plant Cell* **20**, 1134–1151 (2008).

53. J. Negi, *et al.*, A Dof Transcription Factor, SCAP1, Is Essential for the Development of Functional Stomata in Arabidopsis. *Current Biology* **23**, 479–484 (2013).

54. S. Meyer, *et al.*, Malate transport by the vacuolar AtALMT6 channel in guard cells is subject to multiple regulation. *The Plant Journal* **67**, 247–257 (2011).

55. S. Li, *et al.*, Arabidopsis ACYL-ACTIVATING ENZYME 9 (AAE9) encoding an isobutyl-CoA synthetase is a key factor connecting branched-chain amino acid catabolism with iso-branched wax biosynthesis. *New Phytologist* **233**, 2458–2470 (2022).

56. E. Cominelli, *et al.*, A Guard-Cell-Specific MYB Transcription Factor Regulates Stomatal Movements and Plant Drought Tolerance. *Current Biology* **15**, 1196–1200 (2005).

57. M. Hashimoto, *et al.*, Arabidopsis HT1 kinase controls stomatal movements in response to CO2. *Nat Cell Biol* **8**, 391–397 (2006).

58. Y.-K. Liang, *et al.*, AtMYB61, an R2R3-MYB Transcription Factor Controlling Stomatal Aperture in Arabidopsis thaliana. *Current Biology* **15**, 1201–1206 (2005).

59. M. B. Prouse, M. M. Campbell, Interactions between the R2R3-MYB Transcription Factor, AtMYB61, and Target DNA Binding Sites. *PLOS ONE* **8**, e65132 (2013).

60. S. J. Gilmour, *et al.*, Low temperature regulation of the Arabidopsis CBF family of AP2 transcriptional activators as an early step in cold-induced COR gene expression. *The Plant Journal* **16**, 433–442 (1998).

61. Y. Sun, *et al.*, Divergence in the ABA gene regulatory network underlies differential growth control. *Nat. Plants*, 1–12 (2022).

62. S. Heinz, *et al.*, Simple Combinations of Lineage-Determining Transcription Factors Prime cis-Regulatory Elements Required for Macrophage and B Cell Identities. *Molecular Cell* **38**, 576–589 (2010).

63. W. Lahr, K. Raschke, Abscisic-acid contents and concentrations in protoplasts from guard cells and mesophyll cells ofVicia faba L. *Planta* **173**, 528–531 (1988).

64. P.-K. Hsu, *et al.*, Abscisic acid-independent stomatal CO2 signal transduction pathway and convergence of CO2 and ABA signaling downstream of OST1 kinase. *Proceedings of the National Academy of Sciences* **115**, E9971–E9980 (2018).

65. L. Zhang, *et al.*, FRET kinase sensor development reveals SnRK2/OST1 activation by ABA but not by MeJA and high CO2 during stomatal closure. *eLife* **9**, e56351 (2020).

66. M. Dittrich, *et al.*, The role of Arabidopsis ABA receptors from the PYR/PYL/RCAR family in stomatal acclimation and closure signal integration. *Nat. Plants* **5**, 1002–1011 (2019).

67. A. Hiyama, *et al.*, Blue light and CO2 signals converge to regulate light-induced stomatal opening. *Nat Commun* **8**, 1284 (2017).

68. M. Iwafuchi-Doi, K. S. Zaret, Pioneer transcription factors in cell reprogramming. *Genes Dev.* **28**, 2679–2692 (2014).

69. A. Balsalobre, J. Drouin, Pioneer factors as master regulators of the epigenome and cell fate. *Nat Rev Mol Cell Biol*, 1–16 (2022).

70. R. Jin, *et al.*, LEAFY is a pioneer transcription factor and licenses cell reprogramming to floral fate. *Nat Commun* **12**, 626 (2021).

71. S.-K. Han, *et al.*, The SWI2/SNF2 Chromatin Remodeling ATPase BRAHMA Represses Abscisic Acid Responses in the Absence of the Stress Stimulus in Arabidopsis. *The Plant Cell* **24**, 4892–4906 (2012).

72. M. Peirats-Llobet, *et al.*, A Direct Link between Abscisic Acid Sensing and the Chromatin-Remodeling ATPase BRAHMA via Core ABA Signaling Pathway Components. *Molecular Plant* **9**, 136–147 (2016).

73. D. Baek, *et al.*, Histone Deacetylase HDA9 With ABI4 Contributes to Abscisic Acid Homeostasis in Drought Stress Response. *Frontiers in Plant Science* **11** (2020).

74. T. J. Lynch, B. J. Erickson, D. R. Miller, R. R. Finkelstein, ABI5-binding proteins (AFPs) alter transcription of ABA-induced genes via a variety of interactions with chromatin modifiers. *Plant Mol Biol* **93**, 403–418 (2017).

75. L. Song, *et al.*, A transcription factor hierarchy defines an environmental stress response network. *Science* **354**, 1550 (2016).

76. R. Finkelstein, S. S. L. Gampala, T. J. Lynch, T. L. Thomas, C. D. Rock, Redundant and Distinct Functions of the ABA Response Loci ABA-INSENSITIVE(ABI)5 and ABRE-BINDING FACTOR (ABF)3. *Plant Mol Biol* **59**, 253–267 (2005).

77. R. R. Finkelstein, T. J. Lynch, The Arabidopsis Abscisic Acid Response Gene ABI5 Encodes a Basic Leucine Zipper Transcription Factor. *The Plant Cell* **12**, 599–609 (2000).

78. E. Fleta-Soriano, M. Pintó-Marijuan, S. Munné-Bosch, Evidence of Drought Stress Memory in the Facultative CAM, Aptenia cordifolia: Possible Role of Phytohormones. *PLOS ONE* **10**, e0135391 (2015).

79. P. A. Auler, F. B. S. Freire, V. F. Lima, D. M. Daloso, On the role of guard cells in sensing environmental signals and memorising stress periods. *Theor. Exp. Plant Physiol.* **34**, 277–299 (2022).

80. Y. Ding, M. Fromm, Z. Avramova, Multiple exposures to drought “train” transcriptional responses in *Arabidopsis*. *Nature Communications* **3**, 740 (2012).

81. L. Virlouvet, M. Fromm, Physiological and transcriptional memory in guard cells during repetitive dehydration stress. *New Phytologist* **205**, 596–607 (2015).

82. A. van Weringh, A. Pasha, E. Esteban, P. J. Gamueda, N. J. Provart, Generation of guard cell RNA-seq transcriptomes during progressive drought and recovery using an adapted INTACT protocol for Arabidopsis thaliana shoot tissue. 2021.04.15.439991 (2021).

83. A. Lampropoulos, *et al.*, GreenGate - A Novel, Versatile, and Efficient Cloning System for Plant Transgenesis. *PLOS ONE* **8**, e83043 (2013).

FIGURES LEGENDS

Figure 1. ABA induces rapid and genome-wide chromatin remodeling in seedlings. A) Volcano plot of differential ATAC-seq analysis showing regions that significantly change in chromatin accessibility in seedlings after 4hrs of ABA treatment. ABA increased accessibility at 666 regions and decreased accessibility at 214 regions (FDR < 0.001 and FC > 1.5, differential peaks colored in red). **B)** Heatmap of root nuclei ATAC-seq signal (RPKM-normalized) centered over ATAC-seq peaks (+/- 1.5 kb) with ABA-regulated chromatin accessibility during the indicated ABA treatment time course. Across all timepoints, ABA increased accessibility at 1293 regions and decreased accessibility at 1119 regions (FDR < 0.001 and FC > 1.5). **C)** Number of ABA-regulated ATAC-seq peaks over time in roots. ABA-induced peaks are colored in blue while ABA-repressed peaks are colored in pink. **D)** Distribution among annotated genomic features of either all ATAC-seq peaks (orange) or ABA-regulated ATAC-seq peaks (grey). **E)** Genome browser snapshots at two representative genes (*MAPKKK18* and *CML25*) showing changes in ATAC-seq signal in upstream regions following ABA treatment. Scale bars indicate 500 bp. **F)** The transcription factor binding motifs with the highest enrichment (by binomial p-value) in ABA-induced and ABA-repressed chromatin regions in roots.

Fig 2. Cell-type specific epigenomics identifies guard cell specific regulatory elements. A) Left panel is a fluorescence micrograph showing guard cell specific expression of H2B-GFP. Right panel shows a 3D reconstruction from confocal imaging of a 5-week-old *GC1p:H2B-GFP* leaf (merged image shows GFP fluorescence in green and chlorophyll fluorescence in magenta). **B)** FACS analysis of nuclei (DAPI positive) from *GC1p:H2b-GFP* plants. A GFP density plot defines two distinct populations separated by GFP intensity. **C)** DAPI density plot shows that GFP positive nuclei (blue population) are primarily diploid, while GFP negative nuclei (pink population) are distributed over multiple ploidies. **D)** Chromatin accessibility heatmaps comparing ATAC-seq signal (RPKM-normalized) in guard cell, mesophyll, or root cell nuclei. ATAC-seq peaks are separated into guard cell enriched (3272 ACRs), mesophyll enriched (1472 ACRs), and root enriched (3364 ACRs) sets defined by differential accessibility (p.adj < 0.001, Fold-Change > 2). **E)** Principal component analysis (PCA) comparing ATAC-seq biological replicates derived from guard cell, mesophyll, or root nuclei. **F)** A peak-centered ATAC-seq metaplot and a gene-body centered RNA-seq metaplot showing average chromatin accessibility at guard cell specific peaks and average transcript levels of nearest downstream genes (ATAC-seq peak within -2.5 kb and +0.5 kb of transcription start site). Guard cell derived signal is shown in black while mesophyll/leaf signal is shown in green. **G)** Genome browser images displaying ATAC-seq and RNA-seq signal for the indicated tracks near the guard cell expressed gene *KAT1* and the mesophyll cell expressed gene *AOC1*. Scale bars indicate 500 bp. **H)** Results of de novo motif analysis using homer are shown along with the best matching known TFs and the enrichment p-values. **I)** Transcriptional reporter lines generated using cloned guard cell specific ACRs upstream of the genes *AAE9* and *ALMT6,* the positions of the cloned sequences are indicated with orange highlighting on the genome browser images (scale bars indicate 500 bp). Confocal micrographs showing GFP fluorescence (left panel) or merged GFP (green) and chlorophyll (magenta) fluorescence (right panel). Scale bar represents 20 µm.

927 **Figure 3. ABA triggers extensive and persistent chromatin remodeling in guard cells.**
928 **A)** Schematic showing the experimental outline. Plants were sprayed with ABA and infrared images
929 were taken using a thermal camera to assess stomatal closure. Guard cell nuclei were purified at
930 4hrs and 24 hrs after treatment and used for ATAC-seq. **B)** Volcano plot of guard cell enriched RNA-
931 seq data showing that ABA upregulates 2134 transcripts and downregulates 1452 transcripts (FDR <
932 0.001, FC > 2.0). Differentially expressed transcripts are colored in red. **C)** Heatmaps and profile
933 plots of ATAC-seq signal (RPKM-normalized) in guard cell nuclei centered (+/- 1.5 kb) over 2323
934 regions with ABA-induced chromatin accessibility and 1657 regions with ABA-repressed chromatin
935 accessibility (FDR < 0.001, FC > 2.0). The adjacent heatmaps show DAP-seq signal for ABF2 (in
936 red) and AKS1 (in black) centered over the same ABA regulated ACRs, data from (39) and (56). **D)**
937 Comparison of ABA-regulated peaks from 4hr and 24hr timepoints separated ACRs into three
938 categories – early only, sustained (both early and late), and late only. The bar graph shows the
939 number of ABA-increased and -decreased regions in each category. **E)** (Top) Metaplots showing
940 average ATAC-seq signal centered over either ABA-induced or ABA-repressed ACRs and (bottom)
941 RNA-seq metaplots showing average transcript level centered over gene bodies downstream of the
942 same ACRs. Signal from ABA-treated plants is shown in orange and signal from control treated
943 plants is shown in black. **F)** Genome browser images showing guard cell ATAC-seq and RNA-seq
944 signal at a representative ABA-induced gene (*MYB121)* and an ABA-repressed gene (*MYB60*).
945 Scale bars indicated 500 bp. **G,H)** Heatmaps showing TF binding motif enrichments (-log(p-value))
946 in ABA-increased **(G)** and ABA-decreased **(H)** ATAC-seq peaks. **I)** Genome browser images
947 showing guard cell ATAC-seq and RNA-seq signal at the *AKS3* gene. Scale bars indicated 500 bp.
948 **J)** Fluorescence micrograph showing expression of *AKS3pr::GFP-AKS3* in guard cells after
949 treatment with control or ABA (4 hr). **K)** Overlap of ABA-induced accessible regions in guard cell
950 nuclei, mesophyll nuclei, and root nuclei.
951
952
953 **Fig 4. ABF transcription factors are required for ABA-induced chromatin opening in**
954 **guard cells. A)** Heatmaps of ATAC-seq signal (RPKM-normalized) in either *WT* or *abfx4*
955 mutant guard cells centered over 2079 regions with ABA-induced accessibility and 975 regions
956 with ABA-repressed accessibility (FDR < 0.001 and FC > 2.0). ACRs are subdivided by
957 requirement for ABF1/2/3/4 **B)** Overlap of ABA-induced ATAC-seq peaks in *WT* guard cells with
958 those in *abfx4* mutant guard cells. **C)** Genome browser snapshots showing ATAC-seq and
959 RNA-seq signal near two ABA-induced genes *DTX37* and *HSFA6B*. Scale bars indicate 1 kb. **D)**
960 Enrichment (-log(p-value)) of the indicated transcription factor binding motifs in ABA regulated
961 ATAC-seq peaks in either *WT* or *abfx4* mutant guard cell nuclei. **E)** Overlap between ABF DAP-
962 seq peaks and ABA-induced accessible chromatin regions (ACRs). **F)** Peak-centered metaplot
963 showing ATAC-seq signal in the indicated samples at ABA-induced ACRs containing ABF DAP-
964 seq binding sites. **G)** 1000 ABF DAP-seq peaks overlapping ABA-induced ATAC-seq peaks or
965 1000 random ABF DAP-seq peaks were assigned to nearest downstream genes (within -2.5 kb
966 and +0.5 kb of TSS). The plot shows the ABA-induced fold changes within these two sets of
967 downstream transcripts. Asterisks (****) indicate that the distributions are significantly different
968 by Welch's t-test (p < 1E-7) and the red bars represent the means of the distributions. **H)** Bar
969 plots representing the number of ABA-activated or ABA-repressed ACRs over time in *Col-0* or
970 *abfx4* mutant roots.
971
972
973 **Fig 5. ABA and changes in CO_2 concentration induce distinct chromatin remodeling**
974 **programs in guard cells. A)** Diagram showing the effects of different stimuli on the stomatal
975 aperture. **B)** Representative IR image showing differences in leaf temperature due to CO_2
976 induced stomatal movement. **C-E)** Volcano plots of differential ATAC-seq results showing **C)**
977 ABA-regulated chromatin accessibility, **D)** low CO_2 regulated chromatin accessibility, and **E)**
978 high CO2 regulated chromatin accessibility. The numbers of differentially accessible peaks

979 (colored in red, FDR < 0.001 and FC > 2.0) in each condition are indicated on each plot. **F)**
980 Heatmaps and profile plots of guard cell ATAC-seq signal centered over either ABA-regulated
981 ACRs (2079 induced and 975 repressed) or low CO_2-regulated ACRs (329 induced and 487
982 repressed). Libraries are derived from plants exposed to the indicated treatments. **G)** Principal
983 component analysis (PCA) shows that ABA, low CO_2, and high CO_2 introduce separate variation
984 to genome-wide chromatin accessibility. **H)** Genome browser images showing ABA-repression
985 of chromatin accessibility upstream of *HT1*, *BLUS1*, and *CBC1* – three positive regulators of low
986 CO_2 induced stomatal opening. Scale bars indicate 1 kb. **I)** Enrichment (-log P_value) of the
987 indicated transcription factor binding motifs in ABA, Low CO_2, or High CO_2 regulated regions.
988 Negative enrichment scores indicate motifs overrepresented in treatment-repressed regions. No
989 significant enrichment for any of these motifs was found in High CO_2 regulated ACRs.
990
991

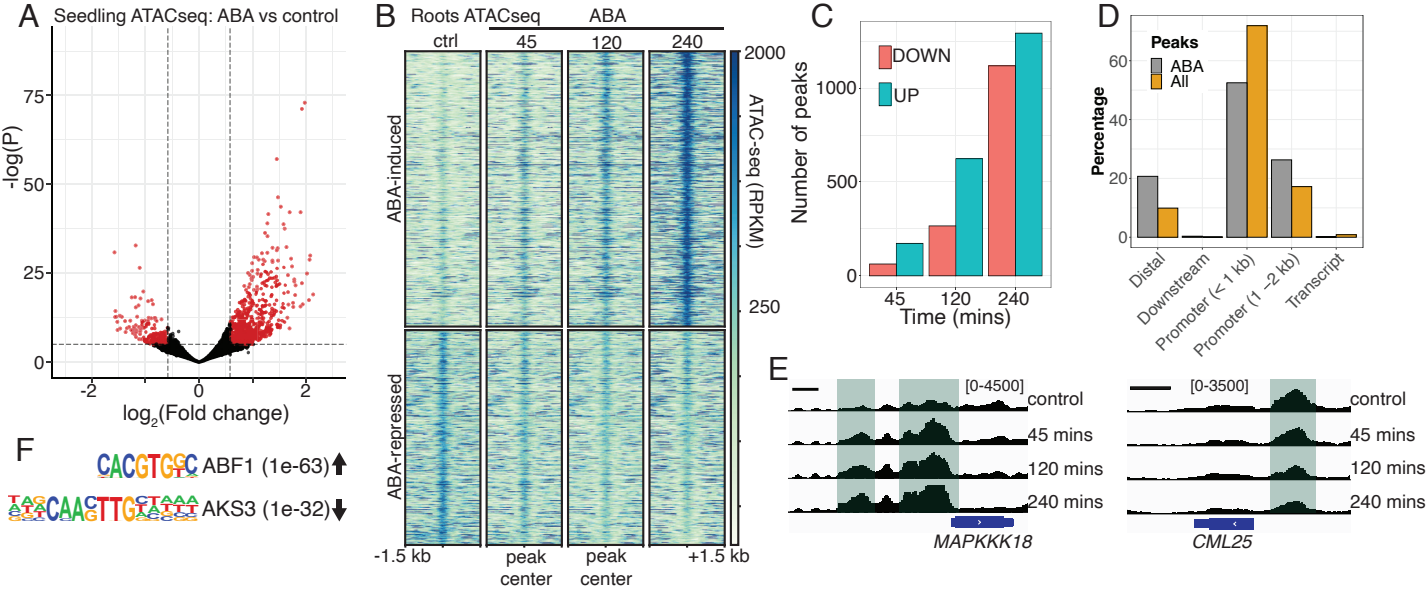
A
Seedling ATACseq: ABA vs control
-log(P)
75
50
25
0
-2
0
2
log2(Fold change)
B
Roots ATACseq
ABA
ctrl
45
120
240
ABA-induced
ABA-repressed
2000
250
ATAC-seq (RPKM)
-1.5 kb
peak center
peak center
+1.5 kb
C
DOWN
UP
Number of peaks
1000
500
0
45
120
240
Time (mins)
D
Peaks
ABA
All
Percentage
60
40
20
0
Distal
Downstream
Promoter (< 1 kb)
Promoter (1 –2 kb)
Transcript
E
[0-4500]
control
45 mins
120 mins
240 mins
MAPKKK18
[0-3500]
control
45 mins
120 mins
240 mins
CML25
F
ABF1 (1e-63)
AKS3 (1e-32)

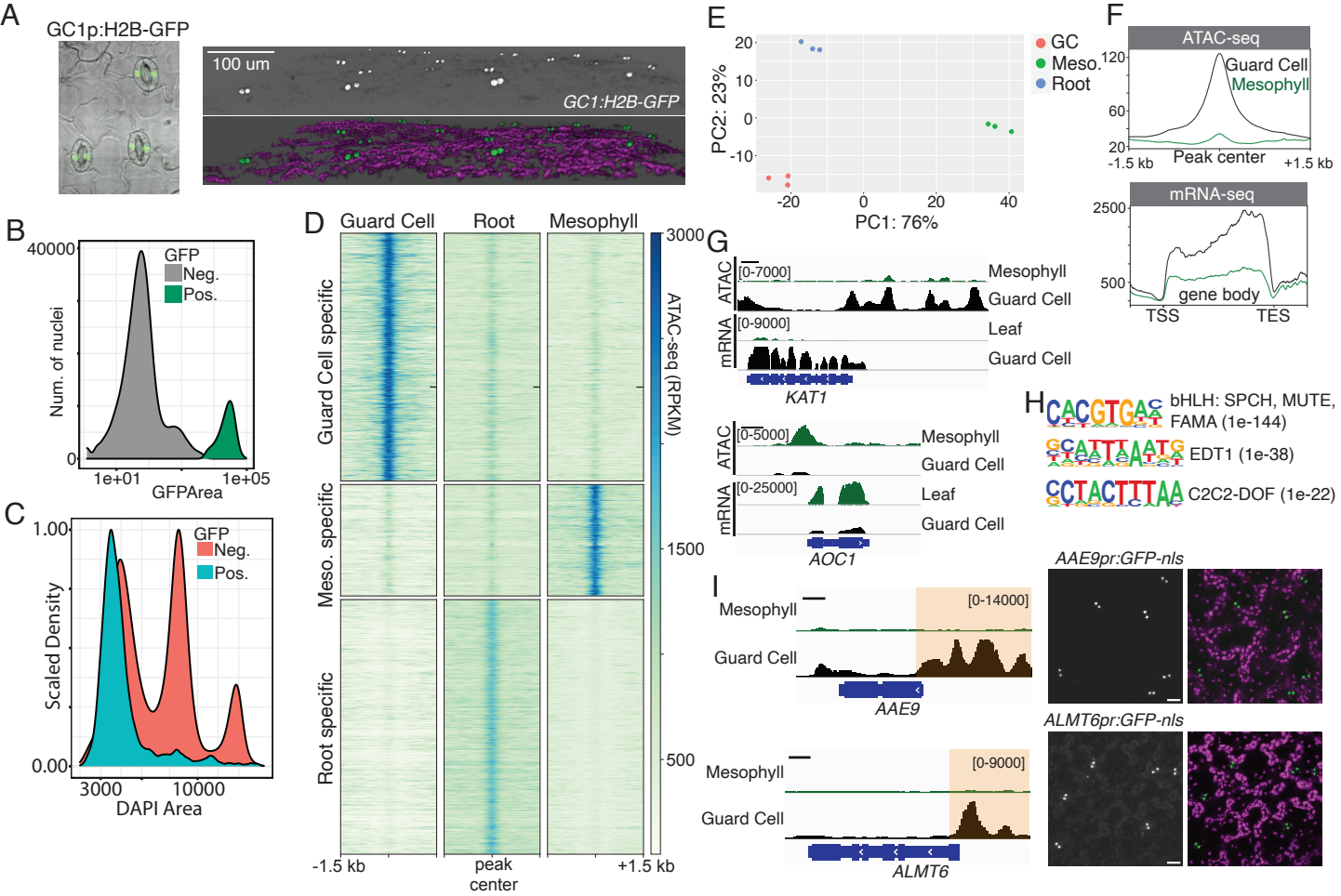
A
GC1p:H2B-GFP
100 um
GC1:H2B-GFP
B
GFP
Neg.
Pos.
Num. of nuclei
40000
0
1e+01
1e+05
GFPArea
C
GFP
Neg.
Pos.
Scaled Density
1.00
0.00
3000
10000
DAPI Area
D
Guard Cell
Root
Mesophyll
Guard Cell specific
Meso. specific
Root specific
ATAC-seq (RPKM)
3000
1500
500
-1.5 kb
peak center
+1.5 kb
E
GC
Meso.
Root
PC2: 23%
PC1: 76%
20
10
0
-10
-20
0
20
40
F
ATAC-seq
Guard Cell
Mesophyll
120
60
20
-1.5 kb
Peak center
+1.5 kb
mRNA-seq
2500
500
gene body
TSS
TES
G
ATAC
[0-7000]
Mesophyll
Guard Cell
mRNA
[0-9000]
Leaf
Guard Cell
KAT1
ATAC
[0-5000]
Mesophyll
Guard Cell
mRNA
[0-25000]
Leaf
Guard Cell
AOC1
H
bHLH: SPCH, MUTE, FAMA (1e-144)
EDT1 (1e-38)
C2C2-DOF (1e-22)
I
Mesophyll
Guard Cell
[0-14000]
AAE9
Mesophyll
Guard Cell
[0-9000]
ALMT6
AAE9pr:GFP-nls
ALMT6pr:GFP-nls

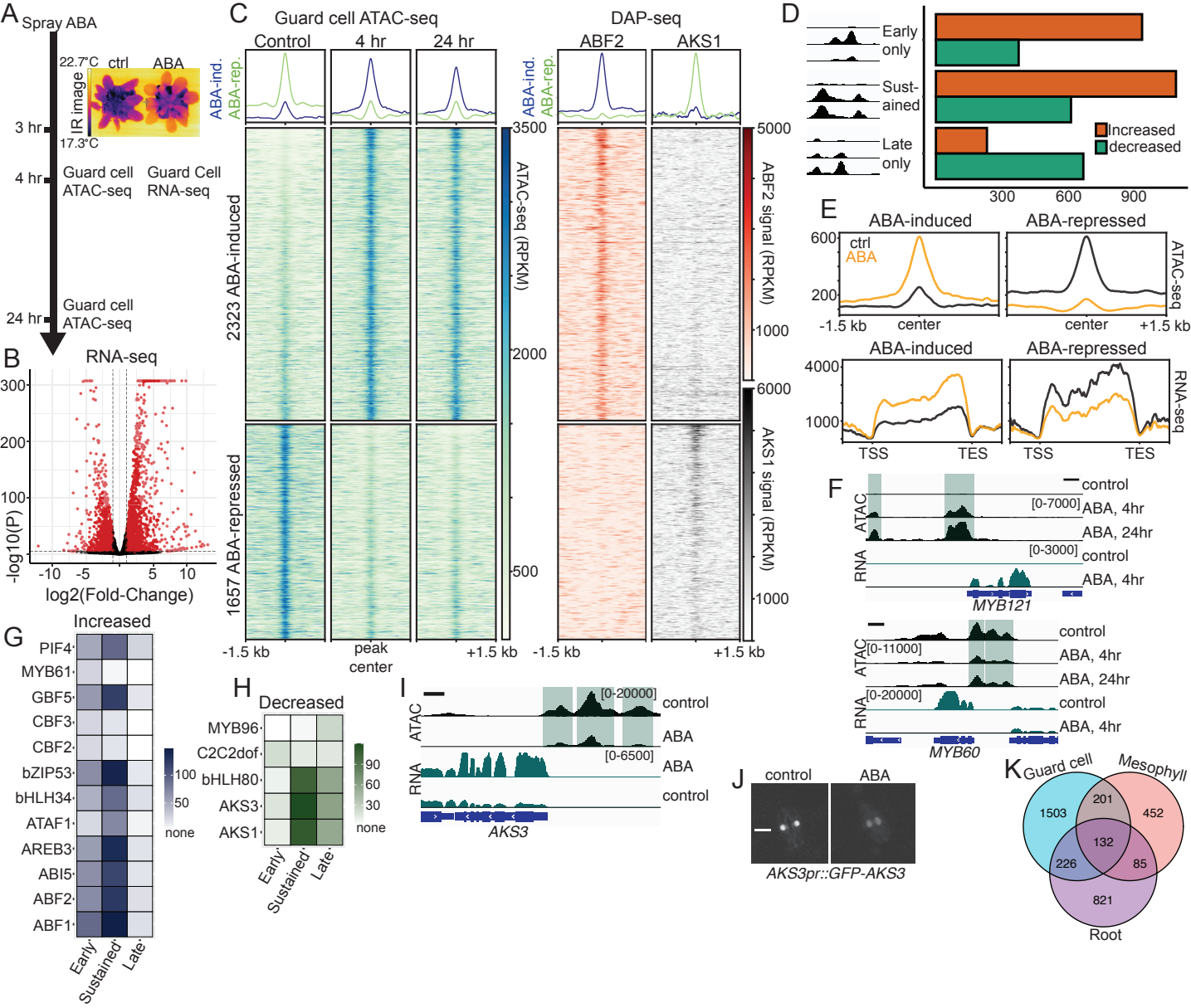
A
Spray ABA
22.7°C
ctrl
ABA
IR image
17.3°C
3 hr
4 hr
Guard cell ATAC-seq
Guard Cell RNA-seq
24 hr
Guard cell ATAC-seq
B
RNA-seq
-log10(P)
log2(Fold-Change)
C
Guard cell ATAC-seq
Control
4 hr
24 hr
DAP-seq
ABF2
AKS1
ABA-ind.
ABA-rep.
2323 ABA-induced
1657 ABA-repressed
ATAC-seq (RPKM)
ABF2 signal (RPKM)
AKS1 signal (RPKM)
-1.5 kb
peak center
+1.5 kb
D
Early only
Sust-ained
Late only
Increased
decreased
E
ABA-induced
ABA-repressed
ctrl
ABA
ATAC-seq
RNA-seq
TSS
TES
F
ATAC
RNA
control
ABA, 4hr
ABA, 24hr
MYB121
MYB60
G
Increased
PIF4
MYB61
GBF5
CBF3
CBF2
bZIP53
bHLH34
ATAF1
AREB3
ABI5
ABF2
ABF1
Early
Sustained
Late
none
H
Decreased
MYB96
C2C2dof
bHLH80
AKS3
AKS1
I
ATAC
RNA
control
ABA
AKS3
J
control
ABA
AKS3pr::GFP-AKS3
K
Guard cell
Mesophyll
Root
1503
201
452
132
226
85
821

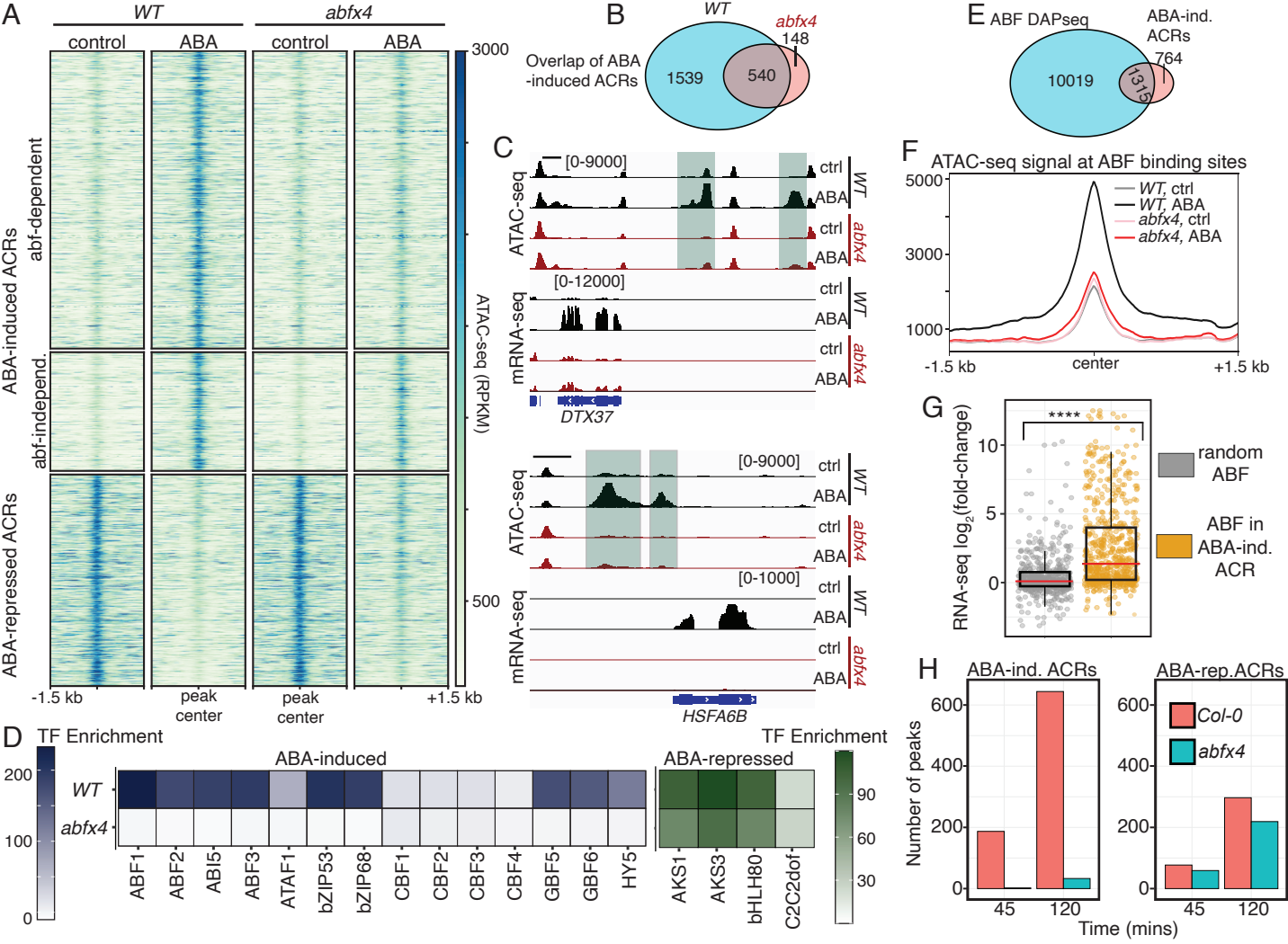
A
WT
abfx4
control
ABA
control
ABA
ABA-induced ACRs
abf-dependent
abf-independ.
ABA-repressed ACRs
3000
ATAC-seq (RPKM)
500
-1.5 kb
peak center
peak center
+1.5 kb
B
WT
abfx4
148
Overlap of ABA -induced ACRs
1539
540
E
ABF DAPseq
ABA-ind. ACRs
764
10019
1315
C
[0-9000]
ATAC-seq
ctrl
ABA
WT
abfx4
[0-12000]
mRNA-seq
DTX37
[0-9000]
[0-1000]
HSFA6B
F
ATAC-seq signal at ABF binding sites
5000
3000
1000
WT, ctrl
WT, ABA
abfx4, ctrl
abfx4, ABA
-1.5 kb
center
+1.5 kb
G
RNA-seq log2(fold-change)
****
10
5
0
random ABF
ABF in ABA-ind. ACR
D
TF Enrichment
200
100
0
ABA-induced
WT
abfx4
ABF1
ABF2
ABI5
ABF3
ATAF1
bZIP53
bZIP68
CBF1
CBF2
CBF3
CBF4
GBF5
GBF6
HY5
ABA-repressed
AKS1
AKS3
bHLH80
C2C2dof
90
60
30
H
ABA-ind. ACRs
ABA-rep.ACRs
Number of peaks
600
400
200
0
Col-0
abfx4
45
120
Time (mins)

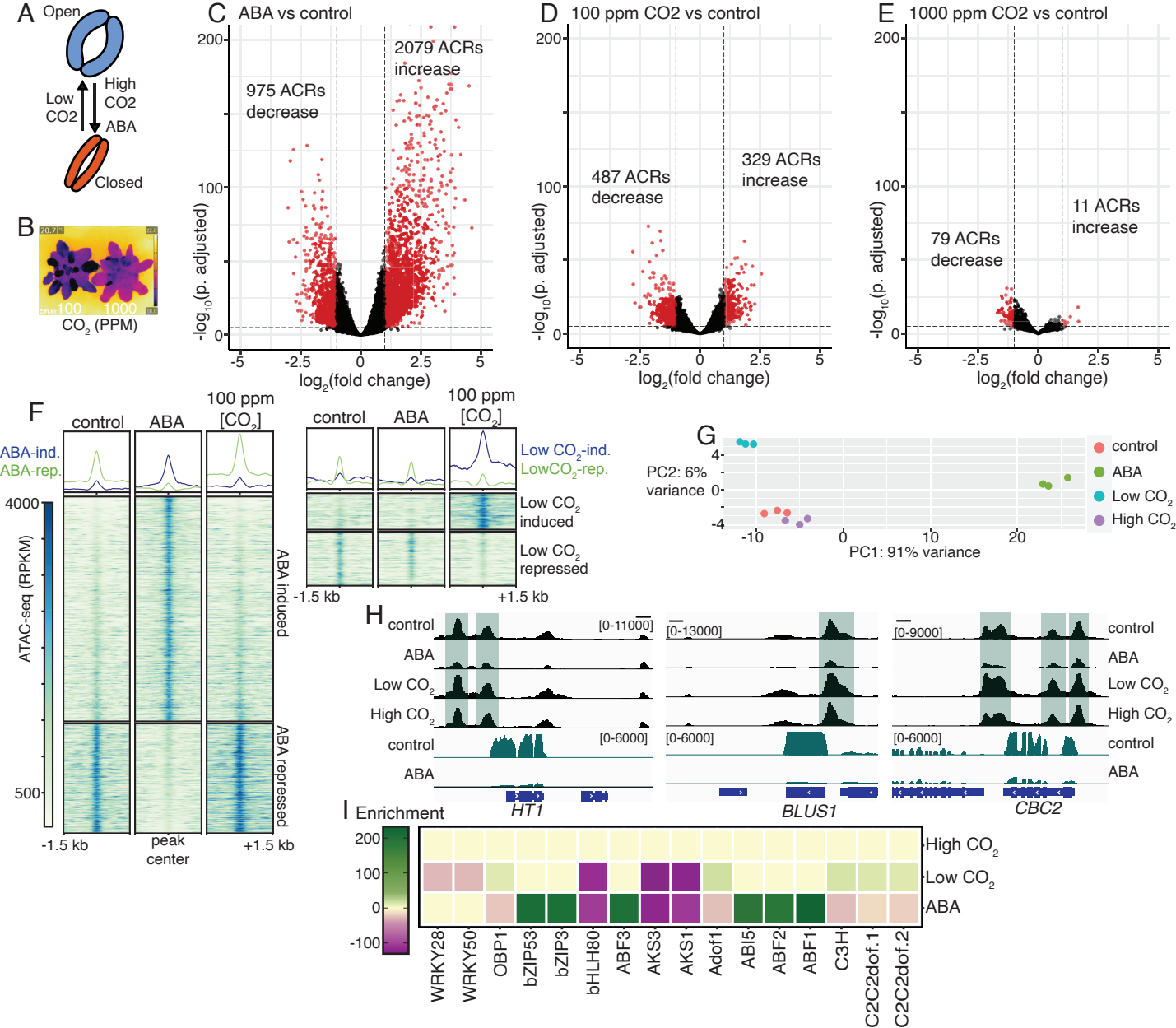
A
Open
Low CO2
High CO2
ABA
Closed
B
100
1000
CO2 (PPM)
C
ABA vs control
975 ACRs decrease
2079 ACRs increase
-log10(p. adjusted)
log2(fold change)
D
100 ppm CO2 vs control
487 ACRs decrease
329 ACRs increase
E
1000 ppm CO2 vs control
79 ACRs decrease
11 ACRs increase
F
control
ABA
100 ppm [CO2]
ABA-ind.
ABA-rep.
ATAC-seq (RPKM)
4000
500
ABA induced
ABA repressed
-1.5 kb
peak center
+1.5 kb
Low CO2-ind.
LowCO2-rep.
Low CO2 induced
Low CO2 repressed
G
PC2: 6% variance
PC1: 91% variance
control
ABA
Low CO2
High CO2
H
[0-11000]
[0-13000]
[0-9000]
[0-6000]
HT1
BLUS1
CBC2
I
Enrichment
High CO2
Low CO2
ABA
WRKY28
WRKY50
OBP1
bZIP53
bZIP3
bHLH80
ABF3
AKS3
AKS1
Adof1
ABI5
ABF2
ABF1
C3H
C2C2dof.1
C2C2dof.2